Latin American Journal of Solids and Structures
www.lajss.org

Experimental and Numerical Investigation of the Dynamic Behavior of Clamped Thin Panel Subjected to Underwater Impulsive Loading

Abstract

The dynamic response and failure mechanism of clamped thin aluminum alloy plates subjected to underwater impulsive loading are investigated by laboratory experiments and finite element (FE) simulations. The effects of plate thickness, impulsive loading and fluid-structure interaction on failure modes in clamped thin aluminum plates are comprehensively assessed in this study. The underwater explosive shock loading experiments were performed by underwater non-contact explosive simulator to identify failure modes of target plates under loads with different intensities. The 3D digital image correlation was applied to measure the real-time deformation of the specimens throughout the impulsive event. Depending on the loading intensity, the failure modes of thin aluminum plates were subdivided into three modes. The Scanning electron micrographs of the fracture surfaces show that the local failure mechanism was tensile necking in all cases. A calibrated FE model was adopted to predict the overall dynamic behavior of plates. The results indicate that the thickness of plates had no significant effect on the deformation modes. In addition, the quantitative relations of plate thickness, the effect of fluid-structure interaction and the failure of plate subjected to underwater shock loading were revealed by the combination of the experimental and simulation results. The results obtained in this research provide a potential guidance to enhance the impulsive resistance of underwater structure.

Keywords

3D digital image correlation; Fluid-structure interaction; dynamic failure; Finite element method; failure mechanism.

Peng Ren [a]
Jiaqi Zhou [a]
Ali Tian [a]
Wei Zhang [b]
Wei Huang [b]

[a] School of naval architecture & ocean engineering, Jiangsu University of Science and Technology, Jiangsu, 212003, P.R. China;
Email: renpeng-hit@hotmail.com, 478355546@qq.com, 75991525@qq.com
[b] Hypervelocity Impact Research Center, Harbin Institute of Technology, Harbin 150080, P.R. China
Email: zhdawei@hit.edu.cn, 748712922@qq.com

http://dx.doi.org/10.1590/1679-78253521

Received 15.11.2016
In revised form 30.03.2017
Accepted 06.04.2017
Available online 20.04.2017

1 INTRODUCTION

The dynamic response and damage mechanisms of structures subjected to underwater impulsive loading play a very important role in determining the viability of marine vessels (Xue and

Hutchinson, 2004). A wide variety of marine structures are susceptible to subject to the high transient dynamic loading from hull slamming, underwater explosions and projectile impacting. These loading can cause severe deformation and damage of submersible structures, and even threat the lives of mariners. The effects of material, the geometric design of structure and fluid-structure interaction (FSI) on blast resistant performance of marine structures must be well known and quantified.

Clamped thin plates are the important components of the structures of the vessel, and a great amount of studies have been carried out about the response of clamped metallic plates subjected to impulsive loading (Langdon, 2014). Menkes and Opat (1973) analyzed the deformation and failure modes of clamped beams subjected to impulsive loading based on experiment results. At a low value of impulse, the beams experienced plastic bending and stretching without rupture, referred to as mode I failure. At an intermediate impulse, the beams stretched in tensile rupture referred to as mode II failure. And at a high value of impulse, shearing off occurring in the beams was referred to as mode III failure. On the basis, Nurick (1991 and 1996) found the same failure modes for clamped plates subjected to impulsive loads. The failure modes of the clamped mild steel square plates were also divided into three phases. The typical discing and petalling failure modes in clamped plates under impulsive loading were analyzed by Lee and Wierzbicki (2005a and 2005b), and the tensile tearing modes were reminiscent mode II of failure modes for beams under impulsive loading. For understanding and improving the blast resistance of rectangular steel plates, Rajendran and Lee (2009) investigated the blast response of the plates to gain greater insight into the damage phenomenon of plates subjected to blast loading. The research of Zamani (2011) indicated that the plastic response of thin metallic plates under explosion loading was very important for designing energy absorbing and collision protection devices. They compared the dynamic response of fully clamped steel and aluminum circular plates subjected to blast loading, and found that the strain rate effect was the essential factor to obtain reasonable results in a theoretical procedure. For developing more experimental researches, Deshpande (2006) and Espinosa (2006) designed the novel experimental methodologies within laboratory to simulate underwater blast shock wave, respectively. On the basis, Espinosa (2006) measured the full deformation fields of plates under underwater blast loading by using the shadow moire and the high speed photography. And then, Latourte (2012) utilized the non-explosive underwater FSI apparatus to study the effect of material mechanical properties on the performance of monolithic steel panels subjected to underwater impulsive loads. Kazemahvazi (2007) investigated the dynamic failure of clamped circular copper plates subjected to underwater shock by experiments and simulations. It is concluded that the failure modes of thin plates were mainly dominated by the peak pressures and independent of the blast wave decay time constant. However, the FSI was not involved in the decoupled algorithm used to calculate the stretching and bending phases of plates in the simulation study. The FSI was one of the important factors for the response and failure of structures (Schiffer et al., 2014). Yuan (2017) also investigated the influence of FSI on the deformation in underwater blast, and the classical problem and the positive effects of FSI were revisited in the fully clamped beam. Hence, more correct analysis and numerical prediction by the coupled algorithm were needed to provide for detailed experimental validation, especially in underwater situation. Meanwhile, a failure mode mapping to identify that the effects of designed parameters on the structural failure mechanism was introduced (Dharmasena et al., 2008). It provided a new perspective to insight into the dynamic response and resistance of structures. For water-backed

plates, the graded effects of metallic foam cores for spherical sandwich shells subjected to close-in underwater explosion were investigated and the arrangement of core: low/medium/high (relative density from the inside to the outside) had the best performance to shock loading (Jin et al., 2016; Yin et al., 2016).

Numerous investigations have been conducted on the dynamic deformation and damage of composite plates subjected to underwater impulsive loading. The research of LeBlanc and Shukla (2011) was focused on the role of laminate attributes on the response of E-glass/vinyl ester curved composite panels subjected to underwater impulsive loading. Then, LeBlanc et al. (2011, 2015) investigated the effects of plate curvature and plate thickness distribution on the deformation mechanism of doubly curved composite panels. Schiffer and Tagarielli (2014a, 2014b, 2015) studied the dynamic deformation of composite plates utilizing a transparent non-explosive underwater shock simulator. The results showed that the composite layup had a minor influence on the blast resistance. Furthermore, Avachat (2014, 2015) analyzed the dynamic deformation and damage response of composites sandwich subjected to underwater impulsive loads and found that shear cracking of front panel and core collapse were the primary failure modes.

The 3D digital image correlation (DIC) is a well-known experimental method to measure the real-time, full-field dynamic deformation of the plates under transient loads such as impact and blast (Sutton et al., 2009). The experimental data could be used to both validate the reliability and the accuracy of the available computational methods and describe the loading and the structural response (Avachat et al., 2014; Zhao et al., 2013). Aune (2016) obtained the response characteristics of thin aluminum and steel plates subjected to air blast loading through the 3D DIC synchronized analyses. Meanwhile, Pinto (2015) validated the accuracy of 3D DIC methodology in the determination of three dimension deflection of a submerged object. They indicated that DIC technique also could be used to study the deformation and failure of air-backed structures subjected to underwater impulsive loading. Although recent advances were focused on the dynamic response and failure of air-backed plates subjected to underwater impulsive loading, a few issues remain to investigate and understand. For instance, the quantified relations between the damage mechanism of plates and the relevant parameters were unclear, such as the relationship of underwater impulsive loading, fluid-structure interaction coefficient and structure parameters to the damage mechanism of plates.

According to the precious research (Huang et al., 2016), the dynamic response of the clamped thin plates subjected to underwater impulsive loading was limited investigated by experimental method. Thus, this paper conducted a combined experimental and numerical study on dynamic response and damage mechanism of clamped thin plates subjected to underwater impulsive loading. The study is focused on describing the dynamic failure of plates and quantifying the deformation of plates as functions of underwater impulsive loading, fluid interaction coefficient and plate non-dimensional thickness to reveal the damage mechanism. Experiments were conducted to obtain the real-time deformation and rupture behavior of the plates by 3D-DIC technique. Furthermore, the 3D finite element simulations based on the full coupling model were performed to validate the experimental results to provide the further understanding about the dynamic deformation and failure mechanism of the monolithic plates. The comprehensive results obtained from the experiments and the simulation presented the damage mechanism of the aluminum plates subjected to underwater

impulsive loading to gain insight into the beneficial characteristics that can be used to design light marine structures.

2 EXPERIMENTAL STUDY

2.1 Experimental Setup and Programme

All experiments were performed at a lab-scaled non-explosive underwater shock loading simulator. The schematic of this apparatus is sketched in Fig. 1. The water tube has an inside diameter of 66mm. The rigid wall of shock tube was applied to confine the expansion of the impulsive wave in a manner that simulates a planar pressure wave. According to the study of Deshpande (2006), the exponentially decaying pressure in water was generated by firing a projectile onto the water piston. The impulse of underwater shock loading was predictable and controlled. The peak pressure and decay time of underwater blast loading were independently adjusted by varying the projectile velocity and mass of the projectile, respectively. A 10mm thick steel projectile (0.2kg) was accelerated by the light gas gun striking the piston to generate the planar impulsive loading. The velocity of projectile was ranged from 20 to 220ms^{-1}, monitored by the laser-velocity gate. The impulsive pressures in water were measured using a high frequency piezoelectric pressure transducer. The pressure transducer included an in-built charge amplifier, an oscilloscope with a rise time of less than 1μs and a resonant frequency above 500 kHz. Hence, the velocity of flyer plate could be used to delineate the effect of loading rate on the deformation and failure behavior of the specimen plates.

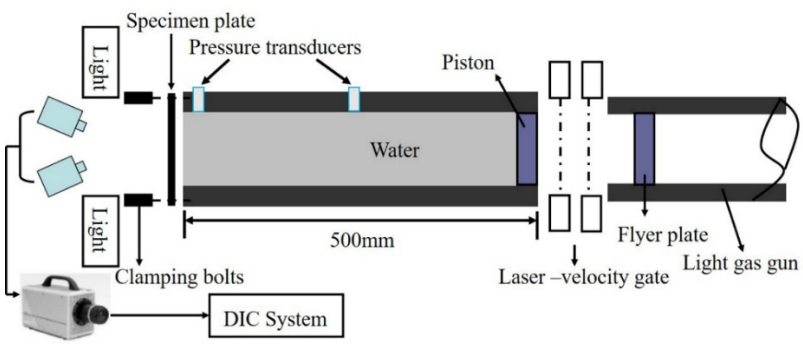

Figure 1: Schematic of underwater impulsive loading apparatus.

In this study, 0.5mm and 2mm thick 5A06 aluminium alloy plates were investigated in tests. The diameter of the circular plate was 152mm, and the diameter of the specimen exposed to the water blast pressure was 66mm.The specimen plate was installed in the end of the water tube with an o-ring, an annular steel clamped ring and six equal spaced bolts. The specimen plate was fully clamped under air-backed through clamping bolts with unsupported middle section, as shown in Fig. 2(a). A number of random flat black speckles were painted to a region covered the entire effective diameter of the specimen plate. The diameter of these circular speckles was painted at least 2mm. Before painting the black speckles, the region of effective diameter was painted white to highlight the black pattern. The picture of the plate painted the random flat black speckles is shown in Fig. 2(b).

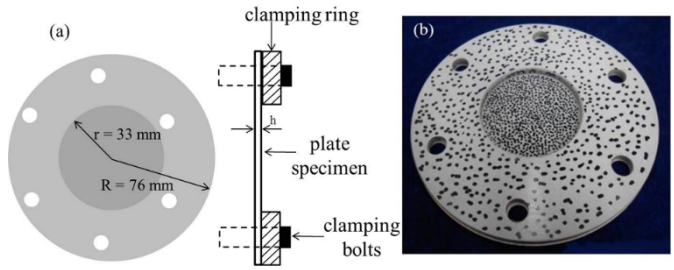

Figure 2: Outline of the specimen plate: (a) Sketch of the specimen long with the side view of the clamping arrangement. (b)The distribution of the random speckles.

Two Photron-Fastcam-SA5 high-speed cameras were used to capture the stereo images of the three dimensional response of specimen plate. The post-processing of these images was performed by the VIC-3D software package to obtain the full-field shape and the deformation measurements. The concrete analysis principle of this technique is shown in Fig. 3. The high speed cameras at 50000 frames per second were set to capture images with an image resolution of 384×384 pixels in all tests and a synchronized trigger device was adopted in the shooting process to ensure the synchronization of two high-speed cameras (Huang et al., 2016). The real-time and full field dynamic response of plate could be determined concretely and clearly by using the 3D-DIC technique.

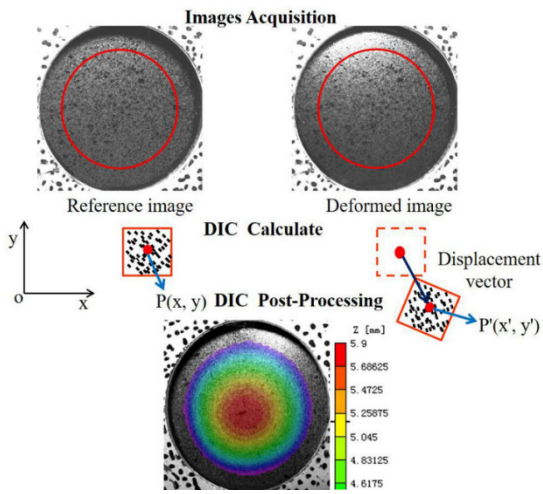

Figure 3: Schematic of the 3D digital image correlation technique.

2.2 Underwater Shock Loading

According to Taylor's analysis of the one-dimensional underwater impulsive waves impinging on the structures (Taylor, 1963), the incident pressure can be idealized as an exponentially decaying relation given by

$$p(t) = p_0 \exp(-\frac{t}{\theta}) \tag{1}$$

Where p_0 is the peak pressure, and θ is the decay constant. Likewise, the impulse impinges onto the clamped plate at normal incidence can be expressed as

$$I = 2\int_0^t p(t)dt = 2p_0\theta \tag{2}$$

The peak pressure and decay time of the impulse wave in the water are dependent on the velocity and mass of the flyer plate, respectively. And the relation can be described in the form as

$$p_0 = c_w\rho_w v_0,\ \theta = m_p/(\rho_w c_w) \tag{3}$$

Consequently, the underwater impulsive loading in this study can be described as the non-dimensional impulse which can be simplified as

$$\overline{I} = I_0/(\rho_w c_w\sqrt{A}) \tag{4}$$

Where c_w is the speed of sound in water, ϱ_w is the density of water, v_0 is the initial velocity of the flyer, mp is the areal mass of the projectile, and A is the area of loading (Deshpande et al., 2006; Espinosa et al., 2006).

3 MATERIAL PROPERTY

The constitutive model of 5A06 aluminum alloy is taken as Johnson-Cook model that accounts the equivalent stress σ_{eq} as a function of effective plastic strain, strain rate and temperature, given as

$$\sigma_{eq} = (A + B\varepsilon_{eq}^n)(1 + C\ln\dot{\varepsilon}_{eq}^*)(1 - T^{*m}) \tag{5}$$

Where ε_{eq} is the effective plastic strain, $\dot{\varepsilon}_{eq}^*$ is the non-dimensionalized effective plastic strain rate, $T^*=(T-T_r)/(T_m-T_r)$ is the non-dimensionalized temperature, T_r and T_m are the reference temperature and melt temperature respectively, A, B, C, n and m are the model parameters (Johnson and Cook, 1985).

According to previous work (Huang et al., 2016), the parameters of 5A06 aluminium based on Johnson-Cook constitutive model are listed in Tab. 1. In addition, the true stress-strain curves of 5A06 aluminum alloy obtained from quasi-static tensile tests are shown in Fig. 4. It is worth noting that the slight oscillations of the curves in Fig. 4 are caused by the machine clamp. According to studies (Kazemahvazi et al., 2007; Ren et al., 2016), the failure strain of metal plate can be assumed to be independent of strain-rate and stress triaxiality. Combined with the stress-strain curves shown in Fig. 4, the 5A06 aluminum alloy plate lost all strength at a material point when the effective plastic strain attained the tensile failure strain $\varepsilon_f = 0.211$ in quasi-static tension tests. Formally, the failure criterion is expressed in terms of damage parameter ω, followed as

$$\omega = \int_0^t \frac{d\varepsilon^p}{\varepsilon_f} \tag{6}$$

Where t is the time when the target plates began to deform. When ω=1, the failure occurs, and the failed element is deleted in the numerical simulation.

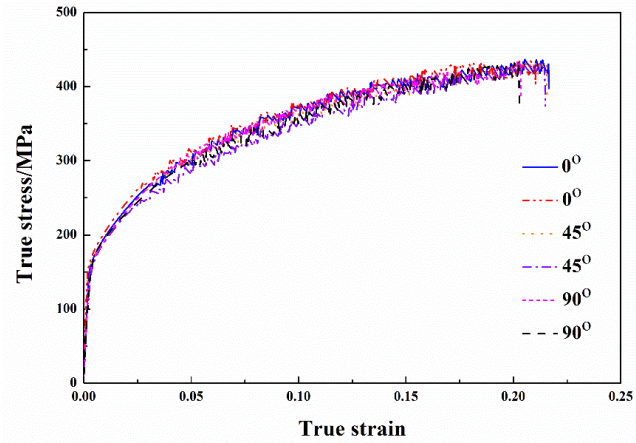

Figure 4: True stress-strain curves at quasi static tensile tests.

E (GPa)	A(MPa)	B (MPa)	C	m	n	ε_f
74	166.97	443.65	0.0223	2.313	0.439	0.234

Table 1: The mechanical property parameters of 5A06 aluminum.

4 EXPERIMENTAL RESULTS

4.1 Pressure Measurements

The pressure histories generated in the water shock tube were measured by the pressure transducers and are given in Fig. 5. The results about the pressure measurements show that the loading was in a reasonable agreement with the characteristics of an idealized underwater blast wave. The decay time of pressure histories measured at 48μs in the experiments was consistent with the theoretical decay time of 50μs according to eq. (3). Hence, it is ensured that the experiments were effective and accurate.

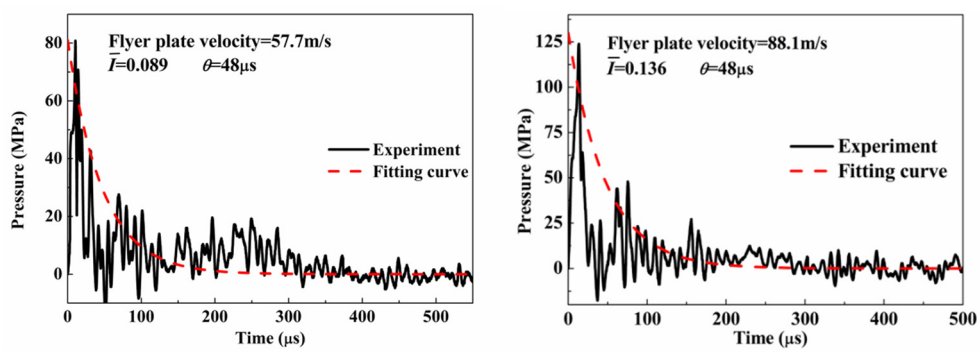

Figure. 5: Experimentally measured histories and corresponding fitting curves.

4.2 Dynamic Deformation Measured by 3D-DIC

During the experimental tests, the 3D-DIC was used to capture the dynamic deformation of the specimens. The sequence of figures in Fig.6 presents 3D topography maps and contours of the transverse displacement field at the characteristic times of the 0.5mm thick specimen subjected to underwater impulsive loading with $\bar{I}$ =0.045. The initial time was corresponded to the time at which the impulsive loading impinges on the plate. It can be observed that the plastic hinge traveled from the periphery to the center of the plate under the fluid-structure interaction, showing as the change of the red area. The highest and ultimate deflection of the middle point was measured at 160μs and 200μs, respectively.

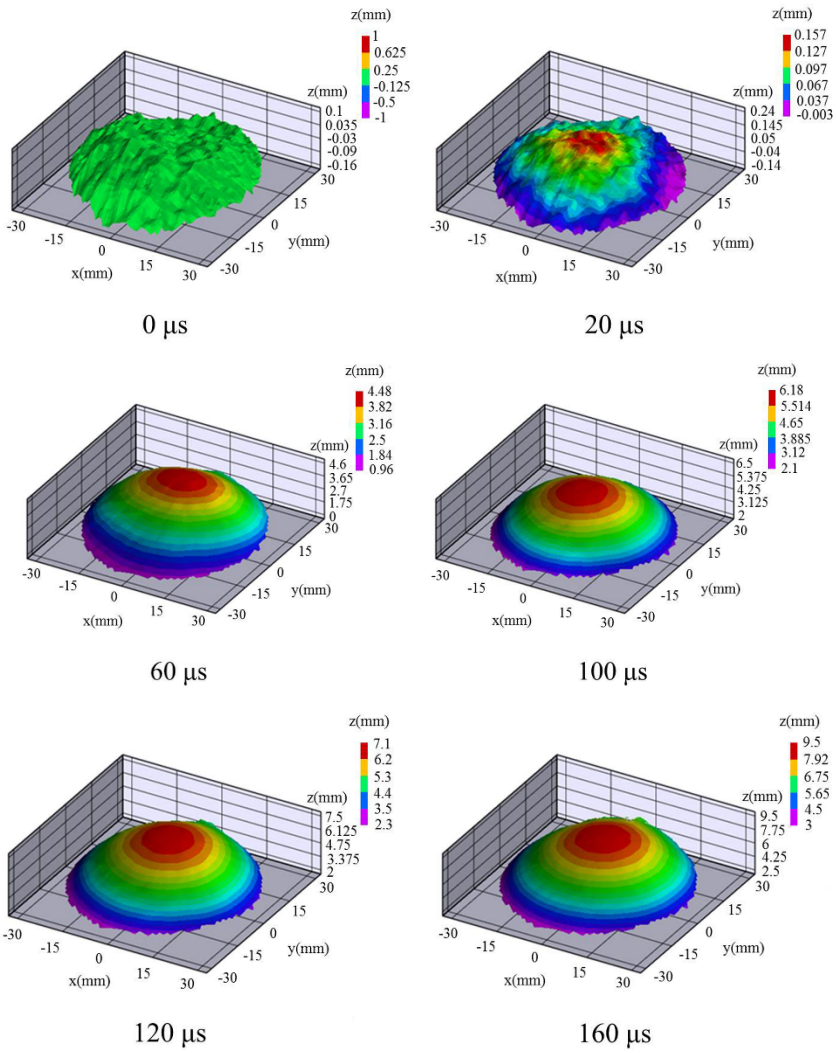

Figure 6: Sequence of the 3D real-time measured photographs showing the out-of-plane displacement in a 0.5mm plate.

The center deflection histories of two different thickness plates were measured in the experiments, shown in Fig. 7 (a). The central histories indicate that the thickness did not affect the deformation tendency of specimen. The maximum deflection of central point increased with the increase of dimensionless impulse. The permanent deformation histories of the 0.5mm plates subjected to two different impulses are plotted in Fig. 7 (b). The comparison of the permanent deformations among plates subjected to different impulses indicates that the loading rates affected the ultimate deformations of the plates and the deformation increased with the increasing impulses. Additionally, Fig.7 (b) expresses that the deformation profiles of the plate recorded by DIC shown in Fig.6 were in a great agreement with the post-test measurements. Hence, it is accurate enough for 3D-DIC to measure the dynamic response of the plates subjected to underwater impulses.

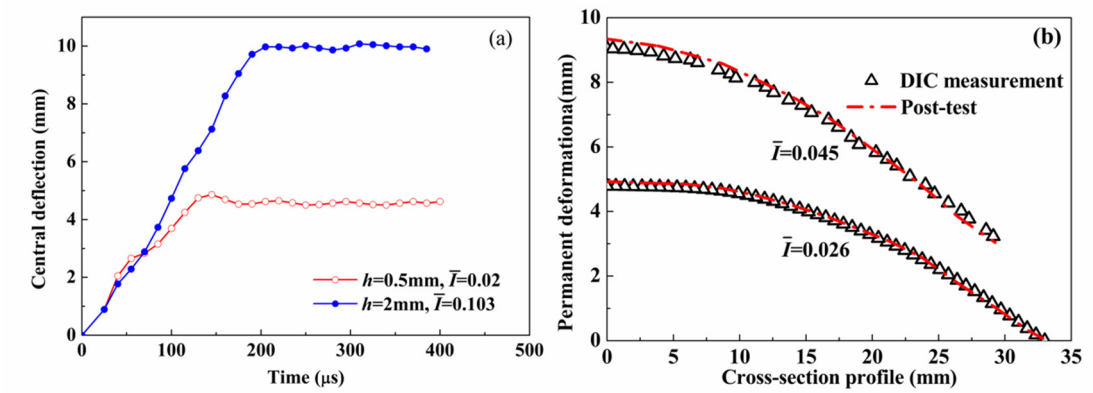

Figure 7: (a) The central deflection histories obtained from experiment, (b) Permanent deformation of 0.5mm-thick plate at different impulses measured by DIC and post-test.

4.3 Typical Dynamic Failure History

The tensile failure (mode II) of the 0.5mm plate subjected to the underwater impulsive loading with $\overline{I}$ =0.088 is shown in Fig. 8. Time t=0 was corresponding to the time at which the impulsive wave impinges on the plate. From the photographic sequence, the plastic hinges traveled from the supports towards the center of the plate before the appearance of a hole, which was similar to the evolution of plate shown in Fig. 6. At 160μs, a hole appeared at the center of the plate, then the crack initiating at the middle of the plate presents four petals after the traveling hinges got final gather.

The shear failure (mode III) history subjected to the underwater impulsive loading with $\overline{I}$ =0.144 is shown in Fig. 9. At 80μs the crack occurred at the supports before the plastic hinges traveling to the mid-span of the plate from the photographic sequence. At 160μs, a shear fracture appeared and stretched along the periphery. And the plastic hinges continued travelling to the mid-span of the plate and finally formed the final deformed shape after the plate had detached from the supports. In addition, the shear failure was not completely symmetrical, because the boundary conditions were not ideal clamped in these experiments.

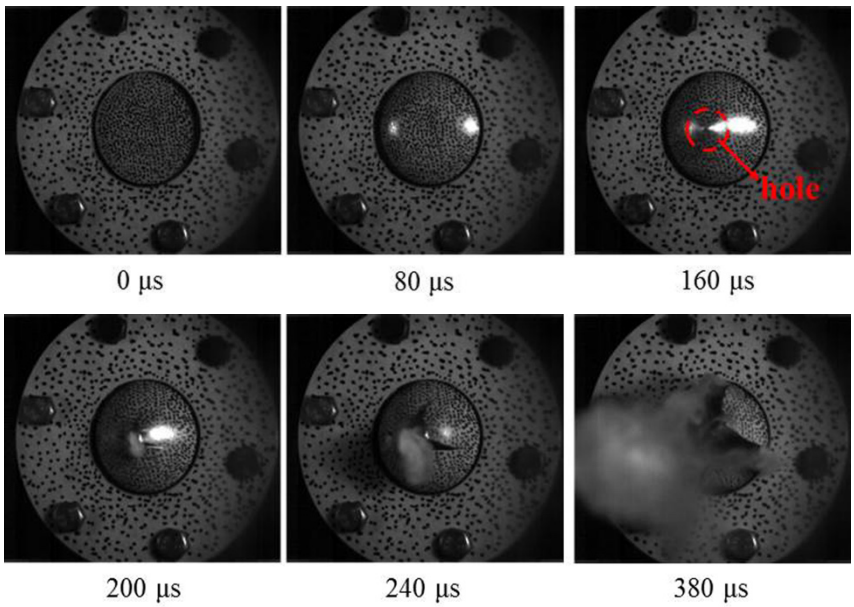

Figure 8: The dynamic failure of 0.5mm plate subjected to the underwater impulsive loading with $\bar{I}$ =0.088 photographed by the high-speed camera.

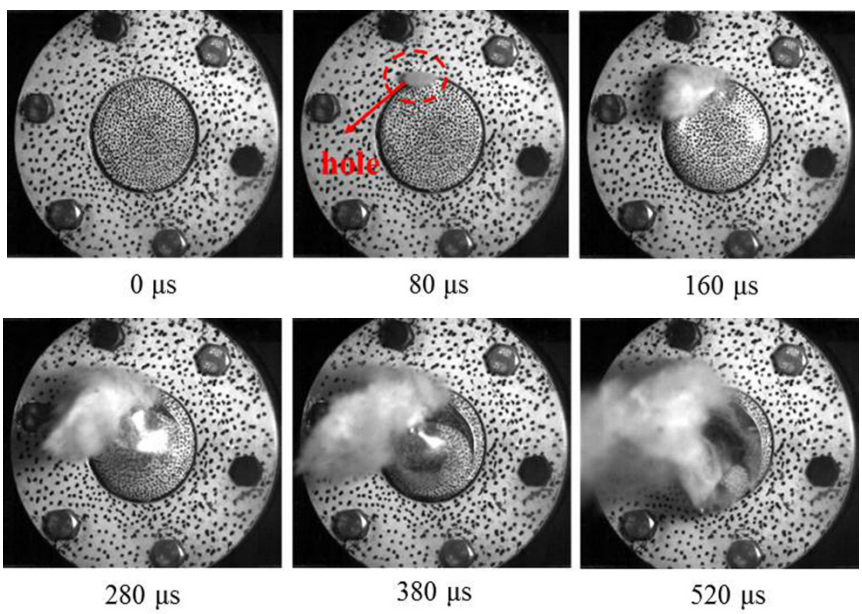

Figure 9: The dynamic failure history of 0.5mm plate subjected to the underwater impulsive loading with $\bar{I}$ =0.144 photographed by the high-speed camera.

The experimental results are summarized and listed in Tab. 2, where h is the thickness of the plate, and p is the peak pressure when the impulsive load impinges on the plate, and δ/R is the midpoint normalized deflection of the specimens. Based on the analysis of Kazemahvazi (2007), the

deformation and failure of aluminum alloy plates were subdivided into three modes from the experimental results. At low impulsive pressures, the plates experienced large plastic deformation and stretched without rupture and this failure was referred to as mode I. At intermediate impulsive pressures, the plates failing in the form of petals due to tensile rupture were referred to as mode II. At high impulsive pressures, shear failure occurred at the supports before the traveling hinges reached the mid-span of the plate, and the final deformation of plate resembled a flat-topped dome. It was labeled as mode III failure. The post-test photographs of several typical failure modes of the aluminum alloy plate are shown in Fig.10.

Exp NO.#	h/ (mm)	p/ (MPa)	$\overline{I}$	(δ/R)max	Failure mode
1	2	34.35	0.038	0.11	I
2	2	61.83	0.068	0.22	I
3	2	93.64	0.103	0.30	I
4	2	139.97	0.154	0.36	I
5	2	172.95	0.191	-	III
6	0.5	18.32	0.020	0.14	I
7	0.5	33.27	0.037	0.27	I
8	0.5	37.41	0.041	0.29	I
9	0.5	40.32	0.045	0.28	I
10	0.5	41.18	0.045	0.37	I
11	0.5	60.40	0.067	-	II
12	0.5	80.13	0.088	-	II
13	0.5	130.15	0.144	-	III
14	0.5	143.14	0.158	-	III

Table 2: Deformation and damage of target plate subjected to different underwater shock loading.

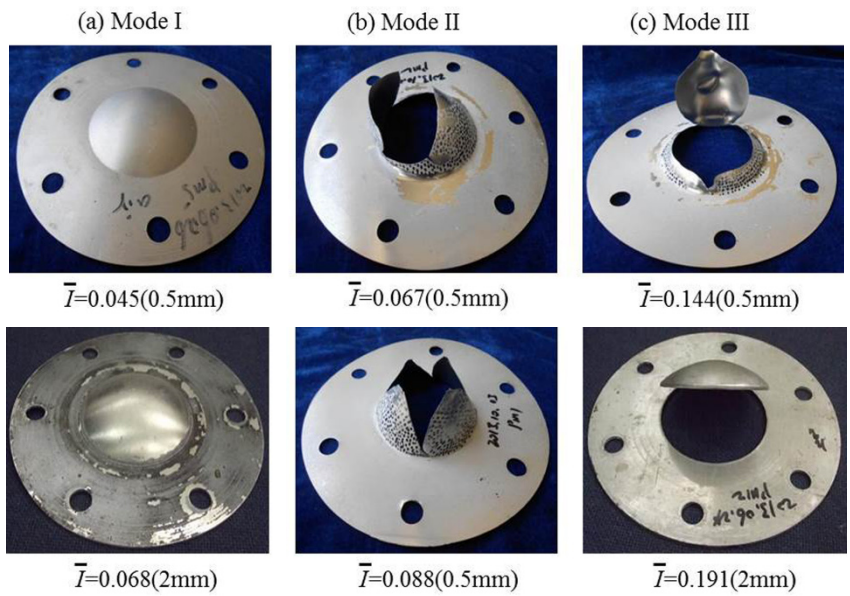

Figure 10: The post-test photographs of three typical failure modes of plates.

Based on the experimental results above, the normalized deflections between 0.5mm-thick and 2mm-thick plates subjected to a set of impulses are shown in Fig.11. It indicates that the deflection of the thinner plates was larger than the thicker plates at the same impulse. Also, the thicker plates experienced longer time of the dynamic response than the thinner ones. It is well worth to notice that the failure points shown in Fig.11 were not the critical values, and just indicated that the plates had failed in mode II or mode III when the impulses reached the failure points.

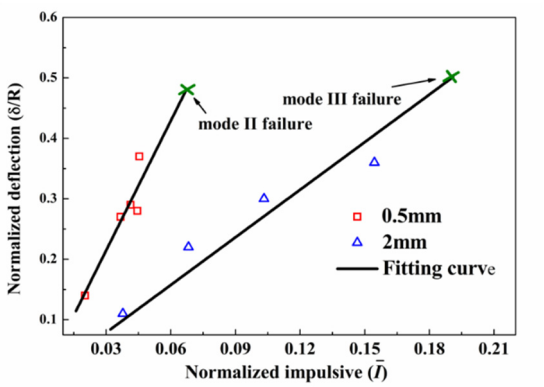

Figure 11: Normalized deflection of 0.5mm and 2mm plates at different impulses.

From the macroscopic failure modes, mode II and mode III were tensile failure by tensile necking at the mid-span of the plate and shear-off near the supports, respectively. Furthermore, the surfaces of the fractures in the microscopic view with electron microscopes were observed in order to examine the failure mechanism of the plate. The scanning electronic micrographs of the different failed surfaces of aluminum alloy plates with 0.5mm thickness subjected to underwater impulsive loading are shown in Fig. 12(a) and (b). It is useful to distinguish whether the failure mechanism in microscopic state was the same as that observed in macroscopic failure modes.

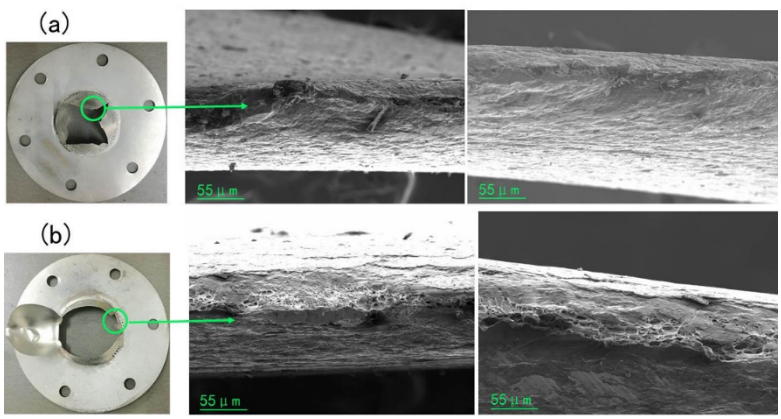

Figure 12: Scanning electronic micrographs of the failed surface of aluminum alloy plates with h=0.5mm subjected to the underwater impulsive loading with (a) $\bar{I}$ =0.088 and (b) $\bar{I}$ =0.144.

The failure of the plate subjected to the underwater impulsive loading with $\bar{I}$ =0.088 was only due to the local tensile necking shown in Fig. 12(a). And the plate subjected to the underwater impulsive loading with $\bar{I}$ =0.144 in Fig. 12(b) failed because of the combined effect of tensile failure and shear failure in microscopic. Hence, it is concluded that all of the thin 5A06 plates experienced the local tensile necking over the entire range of the impulsive pressures from the results of the micrographs of Fig. 12(a) and (b).

Fig. 13(a) shows the load-structure-deformation map of non-dimensionalized deflections (δ/R) of middle points of two thickness plates as a function of non-dimensionalized impulse($\bar{I}$) and thickness(h/R) for all experiments. With thinner thickness and stronger impulse loading, the plates were more susceptible to deform and fail. Subjected to the same impulsive loads, the thicker plates exhibited better deflection resistance. The load-structure-deformation relation was used to obtain the quantified relation among δ/R, h/R and $\bar{I}$. The relation is followed as

$$\delta / R = Z(h / R)^a (\bar{I})^b \tag{7}$$

where Z, a and b are the constants. Fitting the experimental data shown in Fig.13 (b), the constants can be calculated that Z=1.1, a=-0.42, b=1.07. The relation can be quantified by

$$\delta / R = 1.1(h / R)^{-0.42} (\bar{I})^{1.07} \tag{8}$$

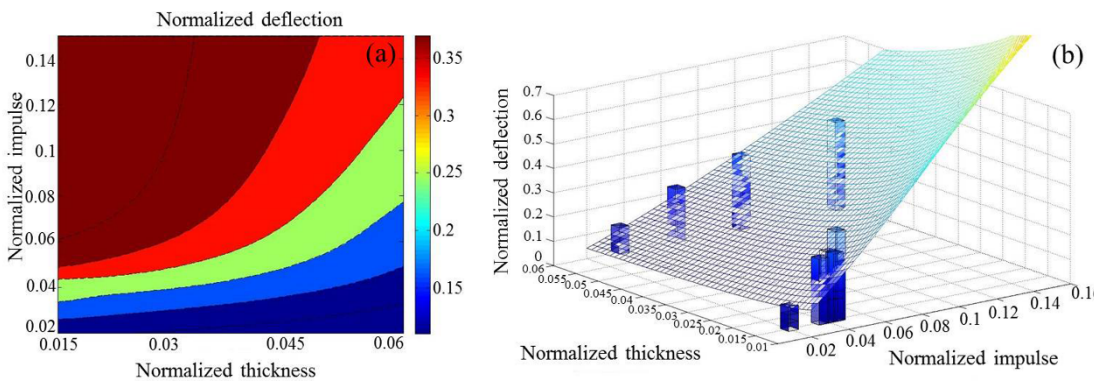

Figure 13: (a) Map of load-structure-deformation, (b) 3D bar picture of experimental data and fitting surface.

5 FINITE ELEMENT SIMULATION

5.1 Numerical Model

The 3D finite element (FE) simulations were performed by LS-DYNA to validate the experimental results and provide the further understanding about the failure modes of the 0.5mm-thick circular aluminum alloy plate. For the reasonable time of calculating, the 1/4 symmetric model was adopted. The finite element model is shown in Fig. 14.

The FE model was consisted of the internal fluid, the shock tube, the piston, the flyer plate and the circular plate. Additionally, the part of air was essential. The sizes of all models were the same as in the experiments, and the mechanical parameters of the 5A06 aluminum are listed in Tab. 1.

The shock tube was simulated in the rigid body and the flyer plate was prescribed with an initial velocity. The shock tube and the outer surface of the plate were held fully constrained in all simulations.

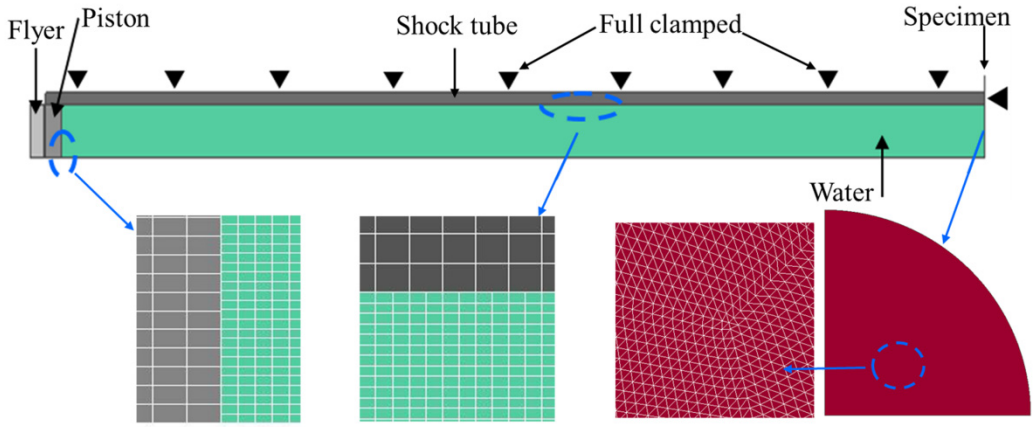

Figure 14: Finite element model.

In this study, the 5A06 aluminum plate was simulated with shell element, and all of the rest structures were simulated with solid element. The fluid and air were simulated with Eulerian meshes in an average size of $1\times0.6\times0.6\text{mm}^3$. The air was modeled to guarantee that the fluid could flow in the meshes when striking the plate. The water and air meshes shared the same nodes at their interface. And the solid structure was simulated with Lagrangian meshes in an average size of $2\times2\times2\text{mm}^3$. Specially, the analysis of Kazemahvazi (2007) showed that the failure predictions of plates were influenced by the mesh size. Hence, the meshes of shell element were chosen triangles with the side length of 0.45mm to ensure the valid numerical simulation for all the failure modes over the entire range of pressures observed in experiments. The above method is called "Arbitrary Lagrangian Eulerian" (ALE) and is often applied to simulate the fluid structure interactions. The ALE element formulation is a criteria numerical approach for simulating the large strain deformation problems, encountering in the metal forming and the high-speed impact applications (Balden et al., 2005). In the basic sense, the ALE method is defined that the mesh motion is independent of the motion of the analyzed material. The greatest advantage of the ALE method is that it allows smoothing of a distorted mesh without performing a complicated remesh. All models comprised of 1660473 elements. The clamping ring and bolts used to clamp the plates to the fixture in the tests were represented by the nodal constraints in the numerical model, shown as the black triangle in Fig. 14. The contact type between the flyer plate and the piston is chosen the Automatic Surface to Surface (ASTS).

The material model of the flyer plate and the piston utilized in this work are *MAT_JOHNSON_COOK. And the material model of both the fluid and air is *MAT_NULL, then the Gruneisen equation of state and linear polynomial equation of state are used to defined the fluid and air, respectively. The parameters of various materials are listed in Tab. 3. As mentioned above that all the thin 5A06 plates experienced the local tensile necking over the entire range of the

impulsive pressures, the failure criterion of largest plastic strain can be applied to the numerical simulation.

Material	ϱ (kg/m3)	A (Mpa)	B (Mpa)	C	m	n	cw (m/ s)	Gruneisen's gamma
Steel	7790	792	510	0.14	1.03	0.26	-	-
Water	998	-	-	-	-	-	1490	0.1

Table 3: Various material properties.

5.2 Numerical Results

5.2.1 Comparison with Experimental Results

The FE simulation has been conducted for the failure mode I of the plate subjected to the impulsive loading with $\overline{I}$ =0.045 in experiment. The dynamic deflection profiles of the plate observed both in the experiment and the simulation are plotted in Fig. 15. The deflection profiles were measured along the diameter of the plate. Time t=0 was corresponding to the time at which the impulsive is impinges on the plate. Compared with the deflection profiles measured by 3D-DIC and the simulation, the deformation over the whole range was in a reasonable agreement. Hence, the FE simulation was accurate enough to predicate the deformation of the plate.

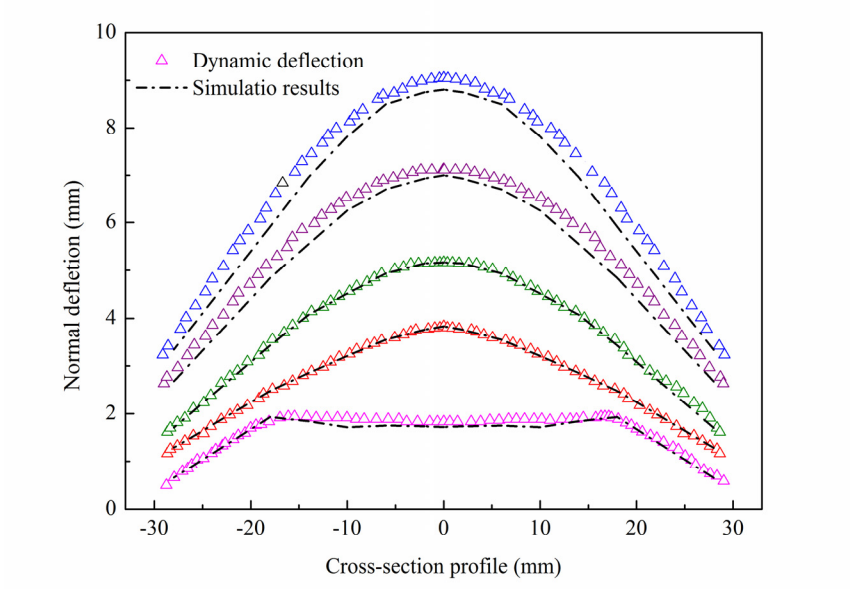

Figure 15: Comparison of the deflections of the plate between the experimental and the simulation.

5.2.2 Pressure History

Fig. 16 shows the sectional view of the impulsive loading with $\overline{I}$ =0.045. Time t=0 was corresponding to the time at which the flyer plate strikes on the piston plate. We can observe from the se-

quence of the pictures that the impulsive waves propagated in the shock tube and impinged on the target plate at the time of 336μs, then the impulsive waves reflected. At the time of 354μs, a part of waves had reflected and the plate had deformed. At 366μs, the impulsive loading was almost counteracted. Hence, it ensures that the plate would not be loaded secondary. In addition, the result indicates that the length of the shock tube used in experiments was reasonable.

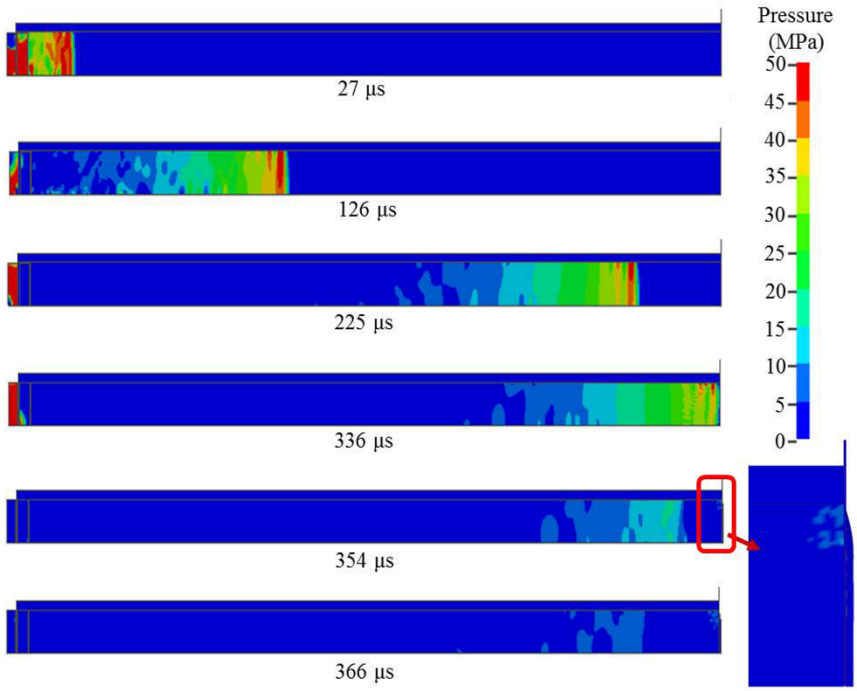

Figure 16: Sectional view of a finite-element simulation showing the distributions of pressure for an impulsive wave with $\bar{I}$ =0.045.

Fig. 17 shows the pressure at different positions distributed along the axis of the water column in the above simulation. When the impulsive wave impinged on the plate, the pressure was decreased quickly and irregularly, because of the cavitation resulting from the fluid-structure interaction. The effect of fluid-structure interaction is regarded as a parameter Ψ and the initial time of cavitaion is τ_c. The relation is followed by

$$\frac{\tau_c}{\theta} = \frac{1}{\psi - 1} \ln \psi \tag{9}$$

where $\psi = \rho_w c_w \theta / m_t$, m_t is the mass per unit area of plate (Taylor., 1963). From this relationship, the theoretical initial time (τ_c) of cavitation is 36μs. Fig. 18 shows the evolution of the cavitation resulting from the fluid-structure interaction. Time t=0 was corresponding to the time at which the impulsive wave impinged on the plate. At 40μs, the cavitation appeared and the phenomenon was in reasonable agreement with the theoretical value. The cavitation zone was grown with the time increasing. After 120μs, the cavitation started to shrink and completely filled with water until 150μs.

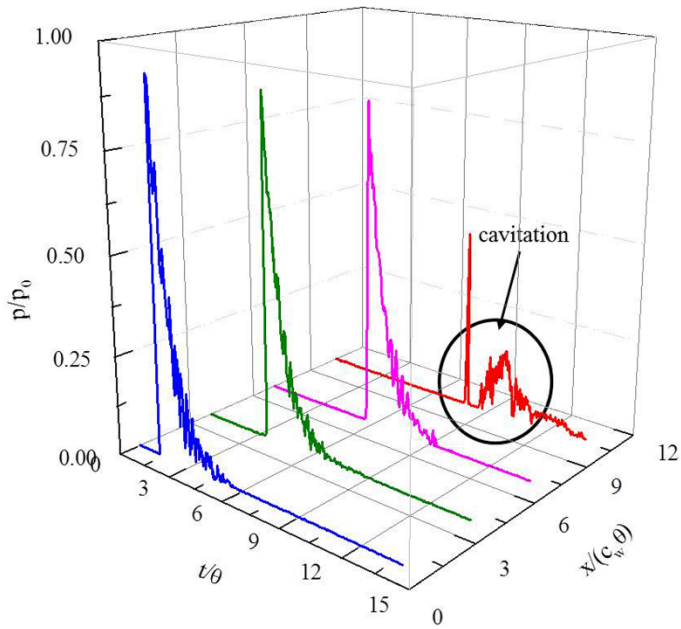

Figure 17: Typical shock tube pressure profile.

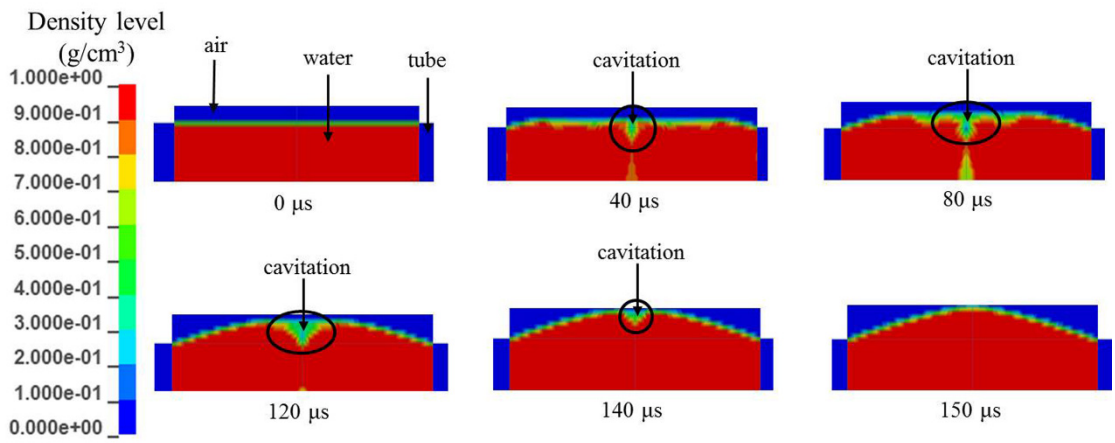

Figure 18: The evolution of the cavitation.

5.2.3 Failure Predictions

Fig. 19 and Fig. 20 show FE predictions about the failure evolution of the plates subjected to impulsive wave with $\overline{I}$ =0.088 and 0.144, respectively. The initial time was that when the impulsive wave impinged on the plate. Compared the failure evolution of the plates shown in Fig. 8 and Fig. 9 respectively, the calculated failure modes of petalling and failure at the periphery of the plates were resembled with the observed modes in experiments. It indicates that the 3D finite element simulations could succeed to predict the dynamic deformation and failure of the plates subjected to impulsive loading.

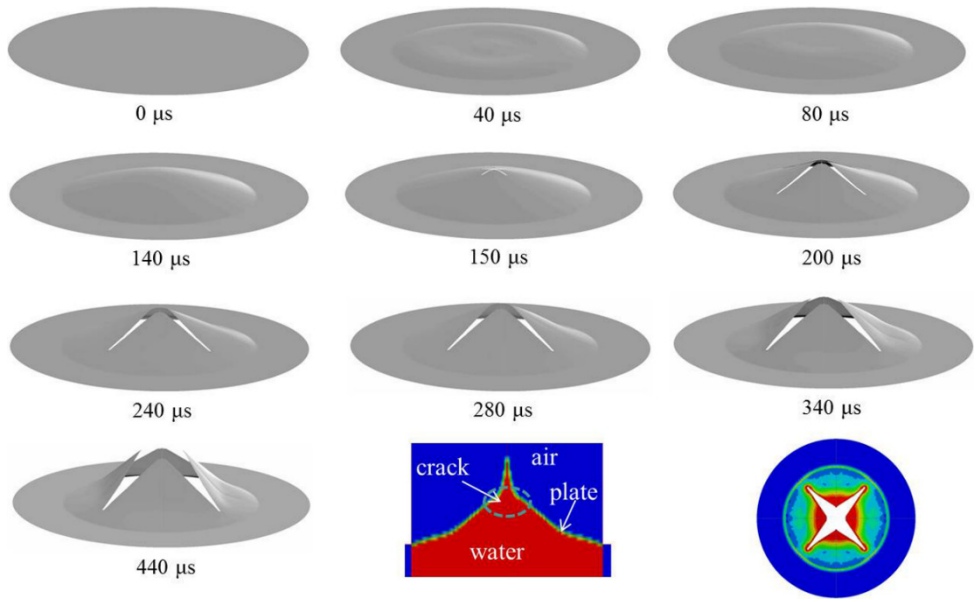

Figure 19: FE calculation of the evolution of the deformation and failure of the plate subjected to underwater impulsive with $\bar{I}$ =0.088 (mode II).

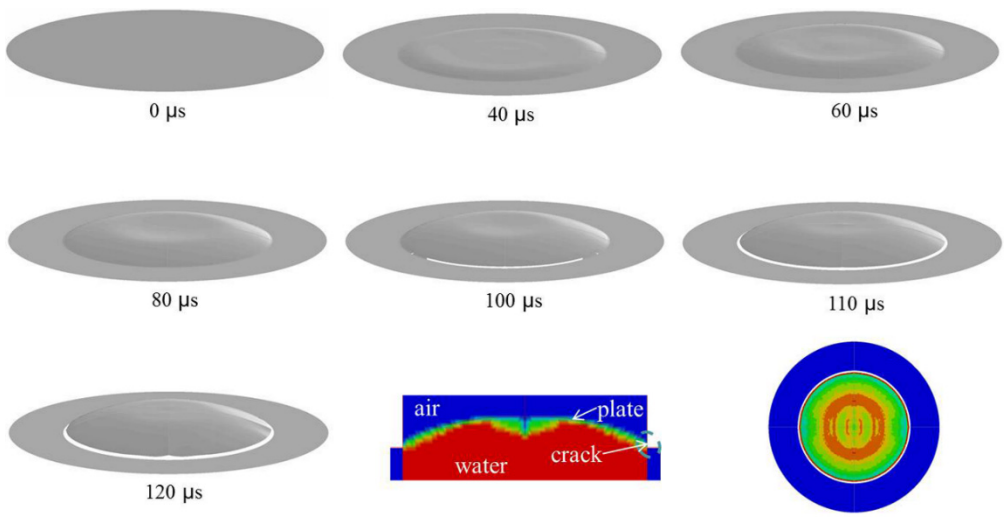

Figure 20: FE calculation of the evolution of the deformation and failure of the plate subjected to underwater impulsive with $\bar{I}$ =0.144 (mode III).

When the underwater impulses reached to the critical values, the failure modes of plates are shown in Fig. 21. As the critical point of failure modes between mode I and II shown in Fig. 21 (a), a sharp was formed at the center of the plate, and the cracks occurred afterwards. Meanwhile, the cracks stopped stretching because of the impulse decreasing. As shown in Fig. 21 (b), the cracks appeared nearly at the same time both at the middle-span and the support of plate. Then, the plate was detached at the periphery with a little tensile rupture at the center of the plate.

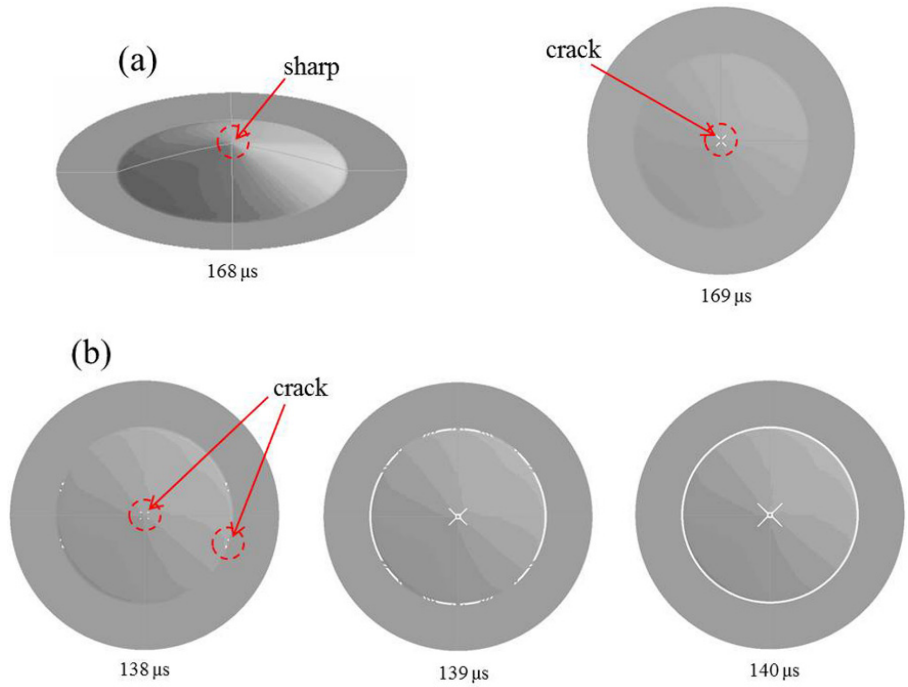

Figure 21: (a) Failure mode of boundary between mode I and II, (b) failure mode of boundary between mode II and III.

5.2.4 Effect of Fluid-Structure Interaction

As mentioned above, the response of the plate was also affected by the fluid-structure interaction. However, the effect of fluid-structure interaction was regarded as the decay time constant and a parameter Ψ. The distribution of three failure modes of 0.5mm 5A06 aluminium plates subjected to underwater impulsive loading is shown in Fig. 22(a) obtained from the FE predictions and experiments, where the σ_s is the yield stress of 5A06 aluminium. According to eq. (3), the decay times of underwater impulsive waves was chosen to be 50μs, 100μs and 150μs, respectively. The critical values between the two failure modes were included in the figure. With the increase of impulse strength, the failure mode of the plate was switched from mode I to mode III. The critical value between mode I and II was less dependent on the change of decay time than that between mode II and III.

According to the three decay times mentioned above and keeping the mass per unit area of plates invariant, the effects of FSI parameter Ψ on the response of the plate subjected to underwater impulsive loads is shown in Fig. 22(b). It can be concluded that the central deflection increased with the FSI parameter and impulsive loading increasing. Additionally, the effect of FSI parameter on the central deflection of the plate was stronger with the impulsive loading increasing. Fitting the experimental data shown in Fig. 22(b), the relation among δ/R, Ψ and $\overline{I}$ is quantified by

$$\delta / R = 13.77\psi^{-0.52}(\overline{I})^{0.459} \tag{10}$$

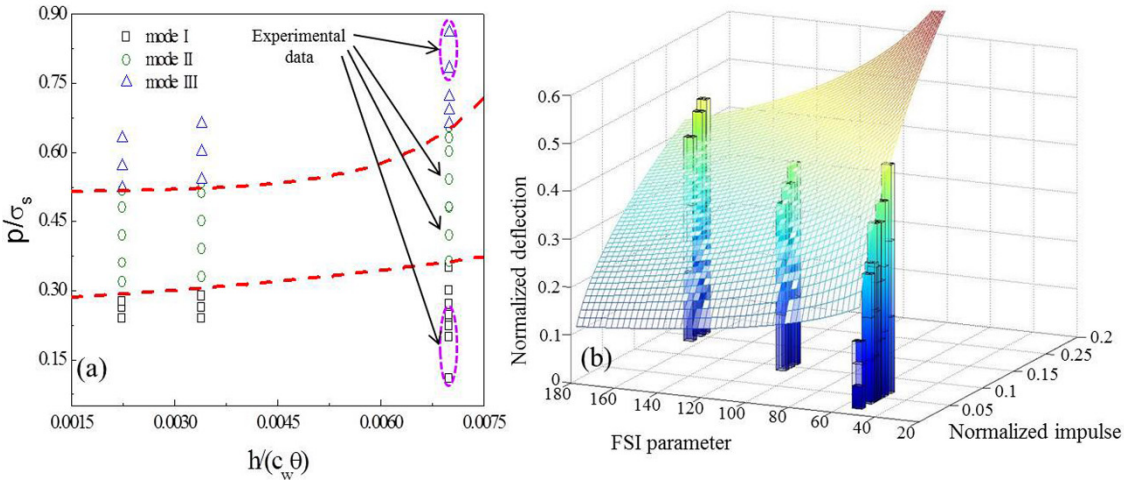

Figure 22: Effect of the fluid-structure interaction (a) the regimes of the three failure modes of specimens, (b) 3D bar picture of obtained data and fitting surface.

6 CONCLUDING REMARKS

The performance of clamped thin aluminum alloy plates subjected to underwater impulsive loads has been comprehensively investigated. From the macroscopic point of view, three modes of deformation and failure were identified in experiments. At low impulsive pressures, the plate experiencing large plastic deformation, bending and stretching without rupture was referred to as mode I. At intermediate impulsive pressures, the plates failed in the form of petals due to tensile rupture and it was referred to as mode II. At high impulsive pressures, shearing failure occurring at the supports and the final deformation of plate resembled a flat-topped dome, which was labeled as mode III. All the failure modes of plates in macroscopic were resulted from the local tensile necking of either petalling or shear-off from the microscopic. In addition, the thicker plates experienced the longer dynamic response than the thinner ones. Hence, the thicker plate exhibited the better deflection resistance subjected to the same impulsive loads. The quantitative relation of plate thickness, impulsive loading and resistance of plate was established in this study above.

A series of the 3D finite element simulations were performed to validate the experimental results and provided the further knowledge about the dynamic response and failure mechanism of the clamped circular aluminum plate. The results of finite element simulation were in good agreement with the observed experimental results. The effects of the fluid-structure interaction on the dynamic response of specimens were studied by utilizing decay time constant of underwater pressure and FSI parameter. The central deflection increased with the FSI parameter increasing. Additionally, the effect of FSI parameter on the central deflection was stronger than the impulsive loading. The critical value between mode I and II was less dependent on the decay time than that between mode II and III. The results obtained in this research provide a potential guidance to enhance the impulsive resistance of underwater structure.

Acknowledgements

The authors are grateful to the National Natural Science Foundation of China (grant No. 51509115); Key Lab Foundation for Advanced manufacturing technology of Jiangsu Province (Grant No. CJ1502); and University Natural Science Research Project of Jiangsu Province (Grant No. 15KJB580005).

References

Aune, V., Fagerholt, E., Hauge, K. O., Langseth, M., Børvik, T. (2016). Experimental study on the response of thin aluminum and steel plates subjected to air blast loading. International Journal of Impact Engineering 90: 106-121.

Avachat, S., Zhou, M. (2014). Response of Cylindrical Composite Structures to Underwater Impulsive Loading. Procedia Engineering 88: 69-76.

Avachat, S., Zhou, M. (2015). High-speed digital imaging and computational modeling of dynamic failure in composite structures subjected to underwater impulsive loads. International Journal of Impact Engineering 77: 147-165.

Balden, V. H., Nurick, G. N. (2005). Numerical simulation of the post-failure motion of steel plates subjected to blast loading. International Journal of Impact Engineering 32: 14-34.

Deshpande, V. S., Heaver, A., Fleck, N. A. (2006). An underwater shock simulator, Proceedings of the Royal Society A 462: 1021-1041.

Dharmasena, K. P., Wadley, H. N. G., Xue, Z. Y., Hutchinson, J. W. (2008). Mechanical response of metallic honeycomb sandwich panel structures to high-intensity dynamic loading. International Journal of Impact Engineering 35: 1063-1074.

Espinosa, H. D., Lee, S., Moldovan, N. (2006). A Novel Fluid Structure Interaction Experiment to Investigate Deformation of Structural Elements Subjected to Impulsive Loading. Experimental Mechanics 46: 805-824.

Huang, W., Jia, B., Zhang, W., Huang, X. L., Li, D. C., Ren, P. (2016). Dynamic failure of clamped metallic circular plates subjected to underwater impulsive loads. International Journal of Impact Engineering 94: 96-108.

Huang, W., Zhang, W., Ye, N., Gao, Y. B., Ren, P. (2016). Dynamic response and failure of PVC foam core metallic sandwich subjected to underwater impulsive loading. Composites Part B 97: 226-238.

Jin, Z. Y., Yin, C. Y., Chen, Y., Hua, H. X. (2016). Graded effects of metallic foam cores for spherical sandwich shells subjected to close-in underwater explosion. International Journal of Impact Engineering 94: 23-35.

Johnson, G. R., Cook, W. H. (1985). Fracture characteristics of three metals subjected to various strains, strain rates, temeratures and pressures. Engineering Fracture Mechanics 21: 31-48.

Kazemahvazi, S., Radford, D., Deshpande, V. S., Fleck, N. A. (2007). Dynamic failure of clamped circular plates subjected to an underwater shock. Journal of Mechanics of Materials and Structures 2: 2007-2023.

Langdon, G. S., Ozinsky, A., Yuen, S. C. K. (2014). The response of partially confined right circular stainless steel cylinders to internal air-blast loading. International Journal of Impact Engineering 73: 1-14.

Latourte, F., Wei, X. D., Feinberg, Z. D., Vaucorbeil, A. D., Tran, P., Olson, G. B., Espinosa, H. D. (2012). Design and identification of high performance steel alloys for structures subjected to underwater impulsive loading. International Journal of Solids and Structures 49: 1573-1587.

LeBlanc, J., Shukla, A. (2011). Dynamic response of curved composite panels to underwater explosive loading: Experimental and computational comparisons. Composite Structures 93: 3072-3081.

LeBlanc, J., Shukla, A. (2011). Response of E-glass/vinyl ester composite panels to underwater explosive loading: effects of laminate modifications. International Journal of Impact Engineering 38: 796-803.

LeBlanc, J., Shukla, A. (2015). Underwater explosion response of curved composite plates. Composite Structures 134: 716-725.

Lee, Y. W., Wierzbick, T. (2005a). Fracture prediction of thin plates under localized impulsive loading. Part I: dishing. International Journal of Impact Engineering 31: 1253-1276.

Lee, Y. W., Wierzbick, T. (2005b). Fracture prediction of thin plates under localized impulsive loading. Part II: discing and petalling. International Journal of Impact Engineering 31: 1277-1308.

Menkes, S. B., Opat, H. J. (1973). Tearing and shear failure in explosively loaded clamped beams. Experimental Mechanics 13: 480-486.

Nahshon, K., Pontin, M. G., Evans, A. G., Hutchinson, J. W., Zok, F. W. (2007). Dynamic shear rupture of steel plates. Journal of the Mechanics of Materials and Structures 2: 2049-2066.

Nurick, G. N., Shave, G. C. (1996). The deformation and tearing of thin square plates subjected to impulsive loads-an experimental study. International Journal of Mechanical Sciences 18: 99-116.

Pinto, M., Gupta, S., Shukla, A. (2015). Study of implosion of carbon/epoxy composite hollow cylinders using3-D Digital Image Correlation. Composite Structures 119: 272-286.

Rajendran, R., Lee, J. M. (2009). Blast loaded plates. Marine Structures 22: 99-127.

Ren, P., Tian, A. L., Zhang, W., Huang, W. (2016). Mechanical property and dynamic response analysis for 5A06 aluminum alloy plates subjected to underwater shock loading. Journal of Vibration and Shock 35: 77-82.

Schiffer, A., Tagarielli, V. L. (2014). One-dimensional response of sandwich plates to underwater blast: fluid-structure interaction experiments and simulations. International Journal of Impact Engineering 71: 34-49.

Schiffer, A., Tagarielli, V. L. (2014). The dynamic response of composite plates to underwater blast: theoretical and numerical modeling. International Journal of Impact Engineering 30: 699-719.

Schiffer, A., Tagarielli, V. L. (2014). The one-dimensional response of a water-filled double hull to underwater blast: experiments and simulations. International Journal of Impact Engineering 63: 177-187.

Schiffer, A., Tagarielli, V. L. (2015). The dynamic response of circular composite plates to underwater blast: experiments and modeling. Journal of fluid and structure 52: 130-144.

Sutton, M. A., Orteu, J. J., Schreier, H. W. (2009). Image correlation for shape, motion and deformation measurements: basic concepts. theory and applications. New York: Springer.

Taylor, G. I. The pressure and impulse of submarine explosion waves on plates. In: Batchelor GK, editor. The Scientific papers of Sir Geoffrey Ingram Taylor. Vol. III: aerodynamics and mechanics of projectiles and explosions. Cambridge: Cambridge University Press; 1963.

Teeling-Smith, R.G., Nurick, G.N. (1991). The deformation and tearing of thin circular plates subjected to impulsive loads. International Journal of Impact Engineering 11:77–91.

Xue, Z. Y., Hutchinson, J. W. (2004). A Comparative Study of Impulse-Resistant Metal Sandwich Plates. International Journal of Impact Engineering 30: 1283-1305.

Yin, C. Y., Jin, Z. Y., Chen, Y., Hua, H. X. (2016). Shock mitigation effects of cellular cladding on submersible hull subjected to deep underwater explosion. Ocean Engineering 117: 221-237.

Yuan, Y., Tan, p. J., Shojaei, K. A, Wrobel, P. (2017). The influence of deformation limits on fluid–structure interactions in underwater blasts. International Journal of Impact Engineering 101: 9-23.

Zamani, J., Safari, K. H., Zamiri, A. (2011). Experimental analysis of clamped AA5010 and steel plates subjected to blast lading and underwater explosion. Journal of Strain Analysis for Engineering Design 46: 201-212.

Zhao, X., Tiwari, V., Sutton, M. A., Deng, X., Fourney, W. l., Leiste, U. (2013). Scalling of the deformation histories for clamped circular plates subjected to blast loading by buried charges. International Journal of Impact Engineering 54: 31-50.